Regular patterns in dichotomically driven activator-inhibitor dynamics

X. Sailer,[1] D. Hennig,[1] V. Beato,[2] H. Engel,[2] and L. Schimansky-Geier[1]
[1]*Institut für Physik, Humboldt-Universität zu Berlin, Newtonstrasse 15, 12489 Berlin, Germany*
[2]*Institut für Theoretische Physik, Technische Universität Berlin, Hardenbergstrasse 36, D-10623, Germany*
(Received 21 December 2005; published 25 May 2006)

We investigate Turing pattern formation in the presence of additive dichotomous fluctuations in the context of an extended system with diffusive coupling and FitzHugh-Nagumo kinetics. The fluctuations vary in space and/or time. Depending on the realization of the dichotomous switching the system is, at a given time (for spatial disorder at a given position) in one of two possible excitable dynamical regimes. Each of the two excitable dynamics for itself does not support pattern formation. With proper dichotomous fluctuations, however, the homogeneous steady state is destabilized via a Turing instability. We investigate the influence of different switching rates (different correlation length of the spatial disorder) on pattern formation. We find three distinct mechanisms: For slow switching existing boundaries become unstable, for high rates the system exhibits "effective bistability" which allows for a Turing instability. For medium rates the fluctuations create spatial structures via a new mechanism where the influence of the fluctuations is twofold. First they produce local inhomogeneities, which then grow (again caused by fluctuations) until the whole space is covered. Utilizing a nonlinear map approach we show bistability of a period-one and a period-two orbit being associated with the steady homogeneous and the Turing pattern state, respectively. Finally, for purely static dichotomous disorder we find destabilization of homogeneous steady states for finite nonzero correlation length of the disorder resulting again in Turing patterns.

DOI: 10.1103/PhysRevE.73.056209 PACS number(s): 89.75.Kd, 05.40.−a

I. INTRODUCTION

The interaction of noise/disorder and nonlinearity has attracted a lot of interest in recent years [1–3]. In particular the possibility of pattern formation induced by fluctuations has been investigated thoroughly [4–11]. There exist various types of underlying dynamics that support spatial structures. Excitability and bistability are among the best studied examples [12].

A prototypical model system exhibiting both of these dynamics is the FitzHugh-Nagumo (FHN) system which we use in the present study. Originally the FHN system was developed to describe nerve cell dynamics [13,14] and afterwards has found applications in many physical, biological, and chemical contexts [15,16]. Spatially extended systems with diffusive coupling that locally obey FHN dynamics have been found to support standing and moving patterns [16,17].

Several of the most prominent patterns observed in nature are due to the Turing instability [1,18,19]. This phenomenon occurs when inhomogeneous perturbations of certain wavelength(s) cause destabilization of a homogeneous steady state.

Fluctuations are omnipresent in nature. Several studies have shown their nontrivial influence on nonlinear systems. Counterintuitively, fluctuations may promote structure formation rather than smear out already existing structures [20].

In a series of recent papers [10,21–23] the possibility of Turing-pattern formation induced by dichotomous fluctuations has been demonstrated. The dichotomous fluctuations switch between two different dynamics each of which does not support Turing pattern formation, i.e., it possesses a pattern-free steady state only. It is the interplay between them that triggers the creation of structures. The authors used dynamical models with either multiplicative dichotomous noise or switched between two distinct dynamics each having its own state dependency.

In the present study we investigate an extended array that locally possesses FHN dynamics that is subject to *additive* dichotomous driving varying either in space or in time or in both simultaneously. Special emphasis is put on the influence of different correlation lengths and times, respectively. Apart from finding Turing structures we also present a mechanism to generate them. It occurs for intermediate correlation times and can thus be distinguished from the previous studies [10,21–23] which operated with small correlation lengths or times, respectively.

More precisely, we illustrate that additive dichotomous switching between two excitable regimes of the individual FHN system may act in the extended system in a way that initially a single local inhomogeneity (single hump on the uniform steady state background) is generated. This inhomogeneity acts as the core from which the pattern evolves throughout the whole space. The growth proceeds stepwise, i.e., with each switching new boundary layers are created adjacent to the core.

The paper is organized as follows. In Sec. II we introduce our noise-driven (extended) FHN system and discuss the dynamics of an individual system. In Sec. III we investigate the effect of purely temporal switchings. We show that there exists qualitatively different behavior for different switching rates. Three different mechanisms create patterns on three different time scales. Although generated by different mechanisms the final patterns are very similar. In order to gain further insight into the pattern formation process we investigate multistability of steady solutions in the *extended* system. To this end we invoke a nonlinear map approach to assure the bistability of homogeneous and Turing pattern states.

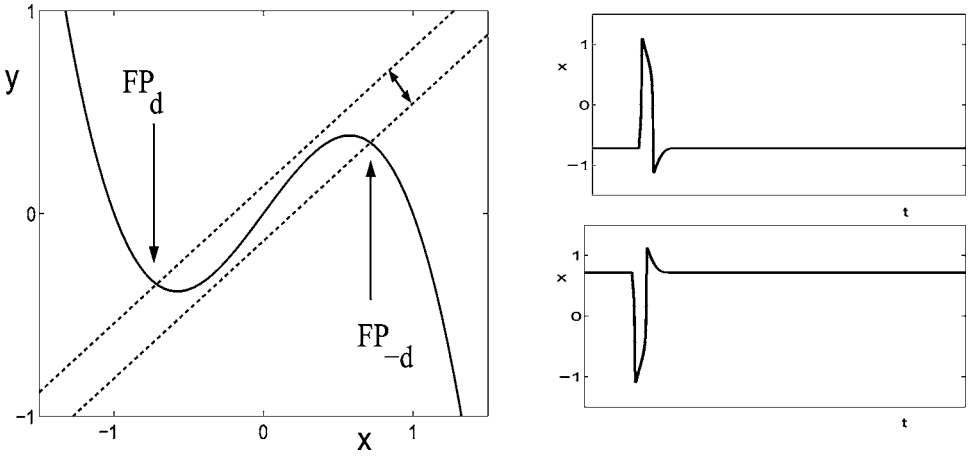

FIG. 1. Nullclines of a single FHN system with solid line: cubic nullcline obtained by setting $\dot{x}=0$, dashed lines: the linear nullcline obtained by setting $\dot{y}=0$. Here the overdot signifies the temporal derivative. The linear nullcline is shown for the two different realizations of the dichotomic driving $I(t)$. FP_i labels the different fixed points. The right hand side shows the dynamics of x for $d=0.2$ (upper plot) and $d=-0.2$ (lower plot) where a superthreshold perturbation has been added and a spike provoked. The dynamics are equivalent but have a symmetry around $x=0$.

Amplitude equations are derived proving subcriticality of the Turing bifurcation. Section IV deals with purely spatial fluctuations. We study the impact of different correlation lengths and find that with their proper choice the parameter range in which a homogeneous steady state is destabilized can be significantly increased. Finally we summarize our results and briefly discuss the influence of fluctuations varying in both space and time.

II. THE DICHOTOMOUSLY DRIVEN FITZHUGH-NAGUMO SYSTEM

We study an extended array with FitzHugh-Nagumo (FHN) kinetics with additive noise obeying the equations

$$\frac{dx_i}{dt} = x_i - x_i^3 - y_i + D_x \Delta x_i, \tag{1}$$

$$\frac{dy_i}{dt} = \epsilon[x_i - a y_i - I_i(t)] + D_y \Delta y_i, \tag{2}$$

where Δ denotes the discrete Laplace operator which in our numerical simulations we treated with the help of the Crank-Nicholson scheme. In what follows we refer to the system (1) and (2) as the lattice system. ϵ is a small parameter ensuring a clear timescale separation of the activator x (fast) and the inhibitor y (slow). Throughout the paper we fixed it to $\epsilon=0.05$. Further, we set the value of a to 1.475 as this value is crucial for the phenomena we present. For the coupling (diffusion) constants we use $D_x=0.02$ and $D_y=5.0$ unless mentioned otherwise. $I_i(t)$ constitutes a random telegraph process which takes one of the two values d and $-d$. We call the rate of the switching between the two states γ. The correlation function $(t_2>t_1)$ of the process is given by

$$\langle I_i(t_1) I_j(t_2) \rangle = d^2 e^{-2\gamma\tau} K(i,j), \tag{3}$$

where $K(i,j)$ is the spatial correlation function between the different sites in the array and $\tau=|t_1-t_2|$.

Before embarking upon a study of the spatio-temporal behavior of the coupled lattice system we consider the dynamics a single decoupled FHN system resulting in the limit $D_x=D_y=0$. Setting additionally $I(t)$ to a fixed value d the system becomes deterministic. For large enough $|d|\left(|d|>d_c=2a\sqrt{\frac{1}{27}\left(1-\frac{1}{a}\right)}\approx 0.104\right)$ the resulting FHN system exhibits excitability. There exists a (single) stable fixed point such that small perturbations in its vicinity decay. On the other hand, perturbations exceeding a certain threshold lead to a large excursion of a unit in phase space before the fixed point is approached again. For $|d|<d_c$ the system exhibits bistability, i.e., it possesses two stable and one unstable fixed point.

Due to the symmetry of Eqs. (1) and (2) under the transformations $x\to -x$ and $y\to -y$ the single system is in another excitable regime with equivalent dynamics for $I(t)=-d$. Thus the switching between the two states of the random telegraph process $I(t)$ entails transitions between two excitable dynamical regimes of the FHN system (1) and (2) associated with either the fixed point located on the left or on the right branch of the cubic nullcline, respectively. A corresponding graphical interpretation is presented in Fig. 1.

III. GLOBAL ALTERATIONS

In assuming spatially uniform driving, i.e., $K(i,j)=1$, global dichotomic switching is applied to the system $[I_i(t)=I(t)]$. We denote by $\dot{\mathbf{x}}_{\pm\mathbf{d}}=\begin{pmatrix}\dot{x}\\ \dot{y}_{\pm d}\end{pmatrix}$ the dynamics of the lattice system (1) and (2) with $\dot{y}$ given by the second equation (2) with $I(t)=\pm d$. The corresponding fixed points are called $\mathbf{x}_{0,+d}$ and $\mathbf{x}_{0,-d}$. $\dot{\mathbf{x}}_{\mathrm{det}}$ stands for the deterministic dynamics arising without driving, i.e., for $I(t)=0$. To gain insight into the impact of the dichotomous switching process on the dy-

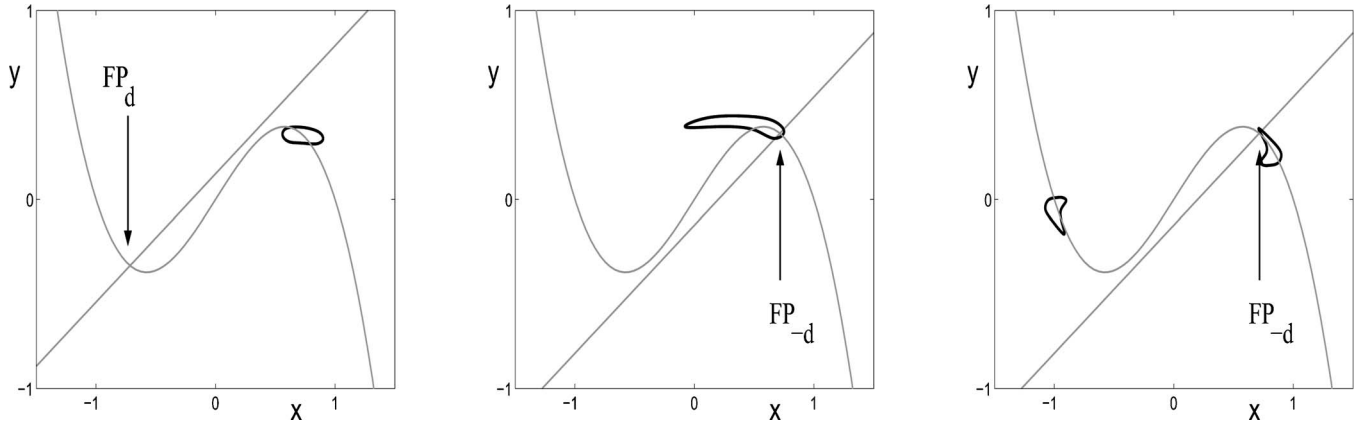

FIG. 2. Development of stationary patterns for medium switching rates in phase space. The system with small inhomogeneities (indicated by a cloud) is initially distributed around a fixed point. Once switching occurs (left panel) the cloud starts to move to the second fixed point. If a second switching occurs just as the cloud is passing from the left to the right (middle panel) it can be split into two. The second cloud then does not return to the fixed point of the deterministic system but moves to the other side where it stays. A spatial structure is formed (cf. Fig. 3, $t=58$).

namics we initialize the system in the dynamical regime $\dot{\mathbf{x}}_{+\mathbf{d}}$ with the initial values of the units $[x_n(0), y_n(0)]$ at one of the fixed points, here taken to be $\mathbf{x}_{0,+d}$. In real space this corresponds to a homogeneous steady state. In our numerical simulations we add tiny but crucial Gaussian white noise of intensity 10^{-6} (for comparison: d is of order 10^{-1}) to the system in order to provide an almost homogeneous distribution of the units around the resting position (hereafter we refer to this set of points with coordinates $[x(t), y(t)]$ as the cloud). Despite its extension in phase space the coupled units in the cloud still represent a virtually homogeneous steady pattern in real space. First we study the dynamic of a one-dimensional (1D) system.

A. Low switching rates

For a very low switching rate γ (so that there is enough time left in between two consecutive switchings that units can travel from one branch of the cubic nullcline to the other) the whole cloud stays at the fixed point $\mathbf{x}_{0,d}$ for a very long time keeping the lattice state close to the homogeneous steady state. Once a switching $d \rightarrow -d$ occurs the

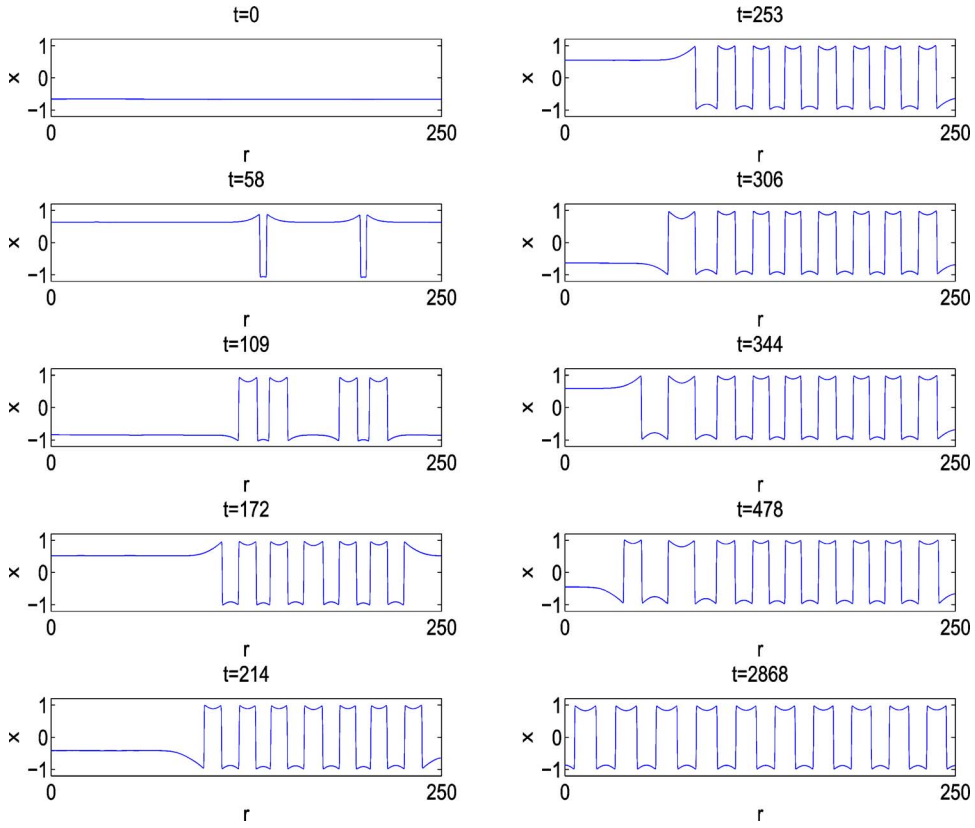

FIG. 3. (Color online) Development of stationary patterns for medium switching rates in real space. After the first nuclei are formed every movement of the homogeneous part of the cloud from one fixed point to the other adds a new layer at either side of the nucleus. After a long time a very regular structure is formed. The time is given above each picture. The y variable (not shown) oscillates with equal period but small amplitude [24]. No-flux boundary conditions are used. The lattice constant is 0.05.

cloud leaves this fixed point for $\mathbf{x}_{0,-d}$ approaching the latter where then all the members of the cloud remain captured in the vicinity of this fixed point until the next switching $-d \rightarrow d$ occurs and the transition process starts all over again.

B. Intermediate switching rates

For higher switching rates γ we find a different behavior: After some time of passage of the complete cloud back and forth between $\mathbf{x}_{0,+d}$ and $\mathbf{x}_{0,-d}$ stationary structures are formed. This behavior is illustrated in Figs. 2 and 3.

The emerging patterns are the product of a switching of the telegraph signal taking place just at the moment when the cloud has begun to cross the excitation threshold. Some individual units of the cloud are already beyond the threshold and, therefore, get excited executing a swift transition to the left outer branch of the cubic nullcline. The remaining units that lag behind, return to the nearby fixed point on the right branch. Those latter units arriving at the left outer branch of the cubic nullcline get trapped there due to the strong inhibitory coupling (vertical direction) that prevents their passage downwards the left cubic nullcline with subsequent return to the right part of the cubic nullcline. This trapping feature, being crucial for the pattern formation, has to be distinguished from the behavior without diffusive coupling, i.e., when $D_x = D_y = 0$. Once an excitable individual unit has made the direct transition from the right outer branch of the cubic nullcline to its left counterpart it runs along the latter until it reaches the minimum of the nullcline. Afterwards the unit departs from the nullcline and performs a straight motion towards its opposite outer branch where eventually the motion terminates at the fixed point. In the corresponding time series of the signal a single spike occurs (see Fig. 1).

In contrast to the uncoupled case, with proper inhibitory coupling (a small ratio D_x/D_y is mandatory) the units that become trapped on the left outer branch of the cubic nullcline arrange their positions such that in real space a large-amplitude spatial inhomogeneity (a hump) is attained. This hump resembles the shape of a localized stationary pattern (also referred to as a "contrast structure" being characteristic for excitable media [17,24–27]. The position on the lattice at which the first hump appears is arbitrary for it depends on that part of the randomly distributed units in the cloud which is beyond the excitation threshold at the switching moment. As was demonstrated in Ref. [25] this stationary pattern is stable with respect to small perturbations. In the appendix we outline a method to obtain stationary localized solutions for the lattice system.

We call such a large spatial inhomogeneity a "nucleus." We stress that a nucleus is extremely robust, that is neither its shape nor its position in real space is affected by further switchings. The homogeneous regions being sufficiently far from the nucleus feel little of it. At each further switching of the homogeneous regions, adjacent to the so far created local spatial inhomogeneities new local humps are built up as is illustrated in Fig. 3. In other words with each switching the inhomogeneous region grows on the expense of the homogeneous region. The formation process goes on adding hump by hump until a periodic pattern covers the whole lattice. Notice the slight deviations in the width of the individual spatial inhomogeneities at early stages of the formation process. Eventually, the diffusive interaction between the neighboring sites leads to the formation of a perfectly periodic pattern. However, it takes diffusion a much longer time to render the pattern regular than it took the pattern to be generated (right lower panel in Fig. 3).

Here we would like to mention that the pattern growth mechanism under random switching (once the first hump has been created) proceeds similar to the one in oscillating media [28]. In fact, in our system the growth behavior observed for periodic switching (not shown) resembles the one observed for random switching.

Here we want to mention that this kind of growth of the inhomogeneous pattern at the boundary layer is due to our choice of parameters. We have performed simulations with different parameter sets and found that it is also possible to add not only one half of a hump at each switching but also three, five, and more halves. (The parameter range for adding simultaneously several layers is very small.) This can, for example, be achieved by a change of the intensity d of the fluctuations. By varying the same parameter it is also possible to substract half a hump with each switching (see Fig. 4). Moreover, a change in the

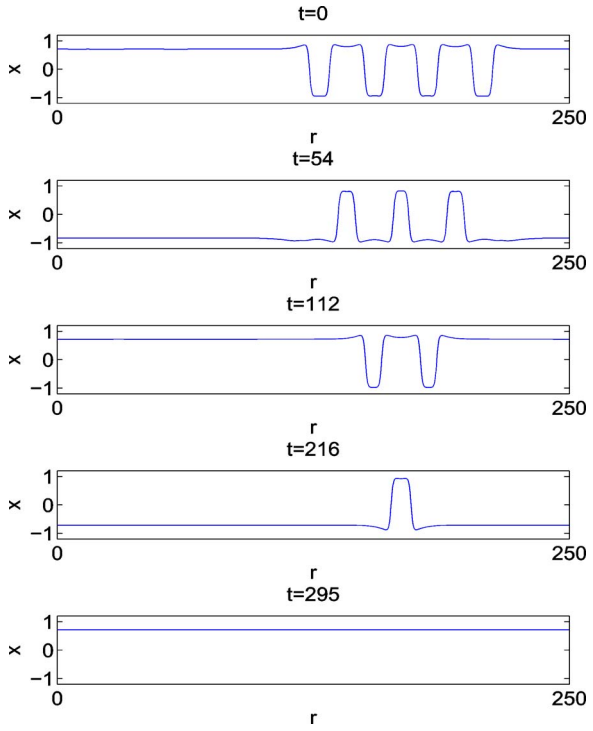

FIG. 4. (Color online) Depending on the parameter values the number of humps can also be decreased ($D_x = 0.9$). Other parameters as throughout the paper. Shown are snapshots shortly after each switching.

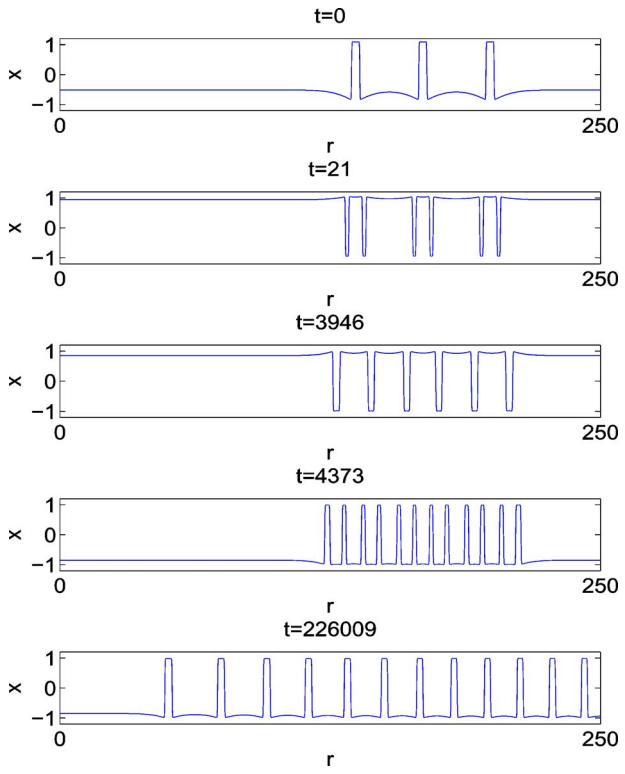

FIG. 5. (Color online) Depending on the parameter values the number of humps can also be multiplied (d=0.5). Other parameters as throughout the paper. In this case the time between two consecutive switchings must be large enough to restore the stable distance between two neighboring humps. Switchings occur only between line one and two and between line three and four.

diffusion constants can double the number of humps in the system (Fig. 5). This multiplier works only for small γ because immediately after the multiplication the distance between two consecutive humps is very small. No new humps fit in between. The time until diffusion has restored the stable distance between them is large. During this time the multiplier does not work. Notice that in contrast to the case treated in Fig. 3 the pattern is not symmetric with respect to $x \to -x$. Let us call the width of a hump (we consider the thin parts as humps; in an infinitely extended regular pattern this choice is arbitrary) l_h and the distance between two neighboring humps Δ_h. Δ_h must roughly increase to three times l_h before a new multiplication can be performed.

The emergence of localized pattern from the homogeneous background can be understood by means of the features of the corresponding stationary system

$$0 = x_i - x_i^3 - y_i + D_x \frac{x_{i-1} - 2x_i + x_{i+1}}{\Delta r^2},$$

$$0 = \epsilon(x_i - a y_i + d) + D_y \frac{y_{i-1} - 2y_i + y_{i+1}}{\Delta r^2}. \tag{4}$$

For the following investigations we set the lattice spacing Δr equal to 1.

By defining

$$x_n = s_n, \quad x_{n-1} = t_n, \quad y_n = u_n, \quad y_{n-1} = v_n \tag{5}$$

the set of equations can be cast into a four-dimensional map form

$$s_{n+1} = \frac{1}{D_x}(-s_n + s_n^3 + u_n) + 2s_n - t_n,$$

$$t_{n+1} = s_n,$$

$$u_{n+1} = \frac{\epsilon}{D_y}(s_n - a u_n + d) + 2u_n - u_n,$$

$$v_{n+1} = u_n. \tag{6}$$

Looking closely at the resulting Turing pattern (lower right panel in Fig. 3) we see that there exist small transition areas between large regions of almost constant amplitude. For an analytic approach we approximate the pattern as bivalued. We will show in the following paragraphs that the map (6) indeed yields bistability of a period-one (P_1) solution (homogeneous pattern) and a period-two solution (Turing pattern).

We are seeking for periodic solutions of Eqs. (6). The period-one solution is quickly found: We set $s_n = s_{n+1}$, $t_n = t_{n+1}$, $u_n = u_{n+1}$, and $v_n = v_{n+1}$ (this means on the lattice: $x_n = x_{n+1}$, and $y_n = y_{n+1}$) and notice that the solutions of the map are equivalent to the stationary solutions of the zero-dimensional FHN model (1) and (2). With our parameters that means that there exists one real valued solution [the value can be found in Eq. (8)].

The procedure is more cumbersome in the period-two (P_2) case: We now set $s_n = s_{n+2}$, $t_n = t_{n+2}$, $u_n = u_{n+2}$, and $v_n = v_{n+2}$ (this means on the lattice: $x_n = x_{n+2}$, and $y_n = y_{n+2}$). We arrive at the following equations:

$$0 = -s_n^3 + \frac{s_n - s_n^3 - u_n}{2D_x} + \left(s_n - \frac{s_n - s_n^3 - u_n}{2D_x}\right)^3 - \frac{(s_n - a u_n + d)\epsilon}{2D_y},$$

$$0 = a u_n - 2s_n - 3d + \frac{s_n - s_n^3 - u_n}{2D_x} + a\left(u_n - \frac{\epsilon(s_n - a u_n)}{2D_y}\right). \tag{7}$$

The real valued solutions of which we can find numerically:

$$P_1: \quad s_n = -0.715, \quad u_n = -0.349, \quad s_{n+1} = -0.715, \quad u_{n+1} = -0.349,$$

$$P_2: \quad s_n = -1.009, \quad u_n = 0.094, \quad s_{n+1} = 0.896, \quad u_{n+1} = 0.099,$$

$$P_2 \quad s_n = -0.842, \quad u_n = -0.218, \quad s_{n+1} = -0.198, \tag{8}$$

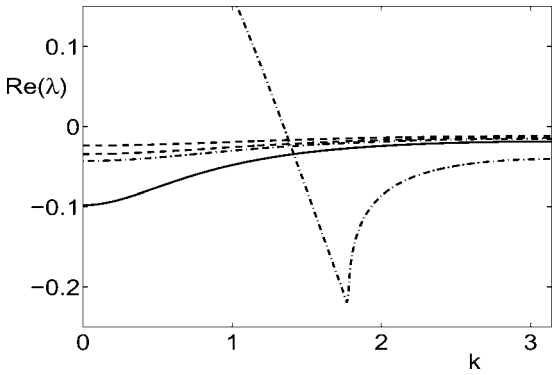

FIG. 6. Real part of the eigenvalue of the linearized problem versus wave vector of the perturbation k. The plot is symmetric to $k=\pi$ and 2π periodic. For better visibility we show only a limited part of the abscissa. The solid line represent the period one solution with $s_n=-0.71526,\ldots$. We see it is stable. The dashed lines represents the period-two solution with alternating sign ($s_n=-1.00925,\ldots$), one line for each fixed point. The dash-dotted lines represent the period-two solution with nonalternating sign ($-0.84286,\ldots$). Parameters $a=1.475$, $\epsilon=0.05$, $d=0.2$, $D_x=0.02$, $D_y=5.0$.

$u_{n+1}=-0.216$.Additional solutions exist with reversed sign as well as with exchanged values of s_n and s_{n+1} and exchanged values of u_n and u_{n+1}. The first solution (upper row) is of period 1. It is the same solution as in the zero-dimensional FHN as discussed above. The second and the third solution are of period two. This fits well to the results from the reaction-diffusion simulation (Fig. 3).

Next we want to test the stability of the solutions. We therefore linearize Eqs. (6) around the fixed points. The corresponding eigenvalue is given by:

$$\lambda(k) = \frac{1-3x_0^2-\epsilon a+2(D_x+D_y)(\cos(k)-1)}{2} + \sqrt{\frac{(1-3x_0^2-\epsilon a+2(D_x+D_y)(\cos(k)-1))^2}{4}-\epsilon}. \tag{9}$$

(There are two eigenvalues for each fixed point. For a stability analysis we need to study only the eigenvalue with larger real part.)

The real part of these eigenvalues is plotted versus the wave number k (by setting $\Delta r=1$ the wave vector k also becomes dimensionless) in Fig. 6. We see that the period-one solution is stable as well as the period-two solution with alternating sign. The other period-2 solution is unstable. Interpreting finite series of humps as a segment of the stable period-2 solution and assuming that such a segment is also stable we can understand the pattern formation in terms of the map orbits: Due to the combined action of the additive noise and the dichotomous switching a finite region of the lattice is brought close to the basin of attraction of such a stable segment. With each further switching the elements at the border of the finite inhomogeneous segment are drawn towards the inhomogeneous solution.

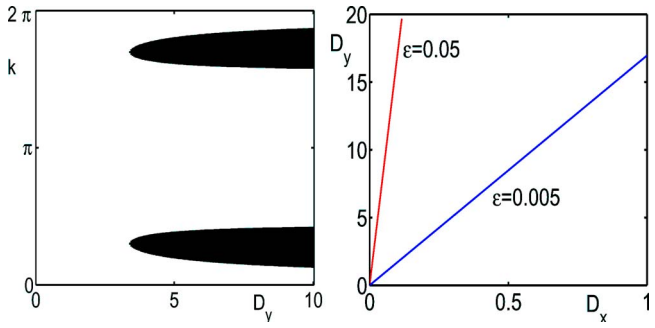

FIG. 7. (Color online) Left: Regions of positive real part (black) of the eigenvalue of the linearized problem in the inhibitor coupling strength-wave vector plane. Other parameters the same as throughout the paper. Right: Region of turing instability for different values of the timescale separation ϵ. The homogeneous state is unstable above the lines.

The proper switching rate at which a local inhomogeneity is created can be estimated as follows: We assume that an individual system ($D_x=D_y=0$) initially sits at the stable fixed point $\mathbf{x}_{0,d}$ and that a switching $d\rightarrow -d$ occurs at time $t=0$. Without further switching and in the limit of perfect time scale separation ($\epsilon\rightarrow 0$) the unit will climb on the cubic nullcline from the $\mathbf{x}_{0,d}$ to its maximum at $x=x_{\max}$. (From there it jumps infinitely fast horizontally to the left outer branch of the cubic nullcline.) The time T it takes for this climbing motion is determined by

$$T=\int_{\mathbf{x}_{0,-d}}^{x_{\max}} dx \frac{1-3x^2}{[(1-a)x+ax^3-d]}. \tag{10}$$

For $a=1.475$ and $d=0.2$ this amounts to $T=0.1107/\epsilon$. Consequently, when its units are distributed around $x=x_{\max}$, the

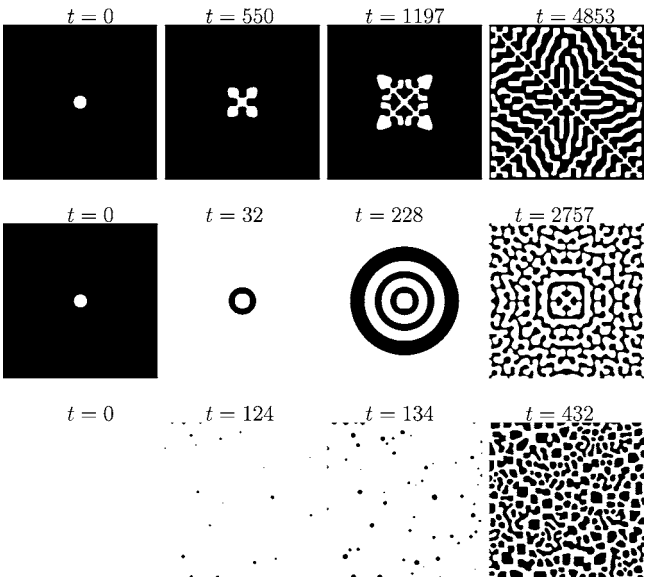

FIG. 8. Time series with different switching rates. The time is given above each plot. Parameters: $\gamma=0$ (upper row), 5.0 (middle row), 0.01 (lower row); $\epsilon=0.05$, $a=1.475$, $D_x=0.02$, $D_y=5.0$, $d=0.2$.

cloud is neither too close to the position of the original fixed point at $\mathbf{x}_{0,d}$ nor is it already in the vicinity of the second one at $\mathbf{x}_{0,-d}$. That the whole cloud now moves as an entity to the left can be prevented if the switching time $1/\gamma$ becomes comparable to T. Suppose the switching $-d \rightarrow d$ has taken place so that the original dynamics $\dot{\mathbf{x}}_{+\mathbf{d}}$ with the fixed point at $\mathbf{x}_{0,d}$ is restored. It is essential for the partition of the cloud that at the instant of switching there is a part of the cloud that is still below the excitation threshold on the right branch of the cubic nullcline as is indicated in Fig. 2. (Note that for the coupled dynamics there is no common excitation threshold valid for all units because whether a system is excited or not depends not only on its own state but also on that of its neighbors.) In fact, then the cloud can break up because those of its units on the forefront with coordinates already beyond the excitation threshold continue the rapid journey onto the left branch of the cubic nullcline while the rest remains on the right branch and gets drawn back by the stable fixed point.

Conclusively, we have demonstrated that global alteration between two different monostable excitable dynamics yields pattern formation while each of the monostable dynamics does not. The situation can hence be viewed as some kind of Parrondo's Game: switching between two loosing strategies constitutes a winning strategy [29].

We underline that the probability per unit time for the occurrence of pattern formation approaches zero as the magnitude of the inhomogeneities (size of the cloud) imposed by the tiny additive Gaussian noise on the system diminishes. Therefore the presence of inhomogeneities is vital for the dichotomously driven mechanism of pattern formation. In general, in any real world system small fluctuations are omnipresent. In our case they are responsible for the extent of the cloud. We also want to mention that the growth of an initial hump occurs also for very low switching rates γ. It takes a much longer time for the phenomenon to occur and we did not observe it in our simulations.

C. High switching rate

We now focus our interest on the limit of a high switching rate γ, i.e., of fast fluctuations. Following Buceta *et al.* [30] we expect such systems to behave as if instead of the signal its temporal average were applied. This is in the present case system (1) and (2) with $I_i(t) \rightarrow \langle I_i(t) \rangle = 0$. For our choice of parameters there exist for a single (uncoupled) system two stable and one unstable fixed points. The stable ones, denoted by $\pm\mathbf{x}_{0,\mathrm{det}}$, are symmetrically placed around the origin of phase space. Clearly, the system with diffusive coupling possesses also fixed points at these locations. However, by choosing proper coupling constants (It is important that the diffusion constant of the inhibitor y is much larger than that of the activator x.) the fixed points may loose their stability via a diffusion induced or Turing instability.

More precisely, the stability of the fixed points $\pm\mathbf{x}_{0,\mathrm{det}}$ depends on the wavelength of the perturbation enforced on the system. The largest eigenvalue $\lambda(k)$ of the extended system linearized around the stable fixed point $\mathbf{x}_{0,\mathrm{det}} = (\tilde{x}\tilde{y})^t$ is given by

$$\lambda = \frac{1}{2}(1 - 3\tilde{x}^2 + \tilde{D}_x + \tilde{D}_y - a\epsilon) + \frac{1}{2}\sqrt{(1 - 3\tilde{x}^2 + \tilde{D}_x + \tilde{D}_y - a\epsilon)^2 - 4(1 - 3\tilde{x}^2 + \tilde{D}_x)(\tilde{D}_y - a\epsilon) - 4\epsilon} \tag{11}$$

with

$$\tilde{D}_{x,y} = 2D_{x,y}[\cos(k) - 1]. \tag{12}$$

In Fig. 7 we show regions of Turing instability in the $k - D_y$ plane. Regions of positive real parts of λ are depicted as black regions. As can be seen perturbations of a finite wavelength larger than zero are favored to grow if the diffusion coefficients are chosen properly. In addition we depict the region where Turing instabilities occur in the D_x-D_y parameter plane for two different values of the timescale separation ϵ. Apparently, with enhanced time scale separation the Turing space is enlarged.

In order to demonstrate the diffusion-induced pattern formation the units of the coupled system are initialized at the fixed point of the deterministic system $\dot{\mathbf{x}}_{0,\mathrm{det}}$ and global dichotomous switching with rate $\gamma = 2000$ is applied. In fact, we find the behavior known from the Turing instability. Small fluctuations grow all over the medium and a very regular periodic pattern evolves. The typical wavelength of this pattern coincides with that of the deterministic nonlinear contrast structure. To verify that the pattern formation is indeed due to the Turing mechanism we reduced the inhibitor diffusion coefficient from our standard value $D_y = 5.0$ to $D_y = 0.5$. In this case the homogeneous pattern persist. Hence, destabilization of the homogeneous steady state is due to the influence of the diffusion.

We demonstrate the effect of different switching rates γ in Fig. 8. For low and intermediate rates we have started with inhomogeneous initial conditions and for high rates with homogeneous ones. Note that inhomogeneities grow due to the combined action of global switching and small additive noise as demonstrated in Fig. 2. In all situations we applied additive Gaussian noise of intensity 10^{-6} to each individual element. The growth of the patterns is due to three different mechanisms. For $\gamma = 0$ the instable border grows slowly into the homogeneous region. In the case of intermediate γ switchings generate additional layers at the boundary. If we denote with L the period length of the final pattern in Fig. 3 we can estimate the speed of the growth of the pattern's

radius as follows. After the time T the process $I(t)$ has on average switched γT times. With each switching an additional layer (half a hump) is appended to the inhomogeneity. The average speed of the propagation of the boundary $\hat{v}$ is then given by $\hat{v}=\frac{1}{2}\gamma L$. This constitutes an upper limit for the average speed because switching have no effect on the growth of the pattern if they occur too early, i.e., before the homogeneous part is in the vicinity of a fixed point. Simulations with different parameter values showed that it is also possible to add instead of one half a layer three, five, or more halves at each side of the inhomogeneity. Also, it is possible to decrease the size of the inhomogeneity. The average speed of propagation is therefore more generally given by

$$\tilde{v}=\left(\frac{1}{2}+Z\right)\gamma L, \tag{13}$$

where Z is an integer number that depends on the parameters of the system (L also depends on the parameters).

For high γ inhomogeneities grow all over the array. The speed with which the patterns grow is therefore different for the three cases: the faster the switching the faster the growth.

D. Weakly nonlinear analysis and amplitude equations

Apparently there exist two distinct steady states namely the homogeneous solution and the periodic (Turing) solution. We surmise that the dichotomous switching constitutes a hard excitation causing the transition between the two states. In order to assure the existence of such a hard excitation we perform a perturbative analysis to derive the amplitude equations describing the evolution near a critical bifurcation point. Note, that we derive the amplitude equations solely for the purpose of showing that there exists a hard excitation in our model.

The homogeneous steady state of Eqs. (1) and (2) in the excitable parameter regime is given by

$$\tilde{x}=\frac{2^{1/3}(a-1)}{(27a^2d+\sqrt{108(1-a)^2a^3+729a^4d^2})^{1/3}}+\frac{(27a^2d+\sqrt{108(1-a)^3a^3+729a^4d^2})^{1/3}}{32^{1/3}a}$$

$$\tilde{y}=\frac{x_0-d}{a}, \tag{14}$$

where d is taken as positive.

For a more convenient treatment we describe the FHN 2 in terms of coordinates relative to the fixed point ($x\to x+\tilde{x}$):

$$\dot{x}=Ax+Bx^2+Cx^3-y+D_x\Delta x,$$

$$\dot{y}=\epsilon(x-ay)+D_y\Delta y \tag{15}$$

with $A=1-3\tilde{x}^2$, $B=-3\tilde{x}$, and $C=-1$.

We briefly outline the linear stability analysis around $(\tilde{x},\tilde{y})$. Imposing small perturbation $u(t)=[\tilde{x}+\delta x(t),\tilde{y}+\delta y(t)]$ yields the linearized equation $(\partial_t-L)u=0$ where L is the linearized operator. The solution of the linearized system can be expanded in normal modes $u=v\exp[\lambda t+ink]$ resulting in the eigenvalue equation $\lambda(k)^2-\mathrm{tr}(L)\lambda+\det(L)=0$ where $\mathrm{tr}(L)$ and $\det(L)$ denote the trace and determinant of the linear operator L, respectively. The condition $\lambda(k_c)=0$ determines the critical wave number at the onset of the Turing instability

$$k_c=\arccos\left(1-\frac{1}{4}\left[\frac{A_c}{D_x}-\frac{a\epsilon}{D_y}\right]\right). \tag{16}$$

We restrict ourselves here to the interval $0\leqslant k<2\pi$. The corresponding critical value of A is given by

$$A_c=\sqrt{\epsilon\frac{D_x}{D_y}}\left[2-a\sqrt{\epsilon\frac{D_x}{D_y}}\right]. \tag{17}$$

A in turn is determined by

$$A(d)=1-3\tilde{x}^2(d), \tag{18}$$

and d plays the role of the control parameter.

To quantify the distance to the critical value the small parameter $\mu=(A-A_c)/A_c$ is introduced. As the next step we derive the amplitude equations to describe the inhomogeneous state beyond linear analysis [31,32]. In our derivation we maintain the discrete Laplacian operator rather than using its continuum differential version. The weakly nonlinear analysis known from the continuum system is then straightforwardly modified to be applied to the lattice system (for details see Ref. [33]). Since just above criticality the eigenvalues of the critical modes are close to zero the assigned modes vary slowly while the remaining noncritical modes relax rapidly. The solution of the linearized equation with wave vector close to k_c can then be expanded as

$$u=\sum_n u_0W_n\exp(ik_cn), \tag{19}$$

where the summation proceeds over the unstable modes and $u_0=\{1,A_c+2D_x[\cos(k_c)-1]\}$ is the eigenvector belonging to the linear operator L. The function W involves the slow time evolution as well as slowly varying spatial changes. Utilizing a standard multiple-scale analysis the control parameter and the solution are expanded in terms of a small parameter $\delta\ll 1$. At each order in δ solvability conditions have to be fulfilled according to the Fredholm alternative. Close to the bifurcation point the critical amplitudes satisfy the amplitude equations in the form of a complex Ginzburg-Landau equation

$$F\frac{dW_m}{dt}=\alpha(W_{m+1}-2W_m+W_{m-1})+\beta W_m+\delta|W_m|^2W_m, \tag{20}$$

with coefficients

$$F=1+\frac{A_c+2\tilde{D}_x}{2\tilde{D}_y-\epsilon a},$$

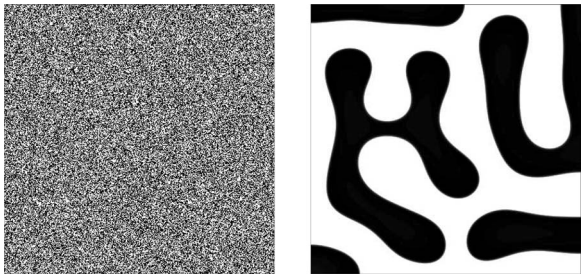

FIG. 9. Turing pattern (right) obtained by applying frozen dichotomic disorder (left) to a homogeneous system at the fixed point. $K(i,j)=\delta_{i,j}$; size: 400×400; $\Delta r=0.1$; $d=0.2$;

$$\alpha = D_x + 2(\cos(k_c) - 1)\left\{ \frac{(A_c + 2\tilde{D}_x)D_y}{2\tilde{D}_y - \epsilon a}[1 + 4D_x] - 4[D_x + (A_c + 2\tilde{D}_x)^2 D_y]\frac{(A_c + 2\tilde{D}_x)D_y + 2\tilde{D}_y - \epsilon a}{\epsilon a + (2\tilde{D}_y - \epsilon a)(A_c + 2\tilde{D}_x)^2 D_y} \right\},$$

$$\beta = A - A_c,$$

$$\delta = 2B\left[\frac{2aB}{1 - aA} + \frac{(\epsilon a - 2\tilde{\tilde{D}}_y)B}{\epsilon - (\epsilon a - 2\tilde{\tilde{D}}_y)(A_c + 2\tilde{\tilde{D}}_x)} \right], \quad (21)$$

with the abbreviations

$$\tilde{D}_{x,y} = 2[\cos(k_c) - 1]D_{x,y}, \quad \tilde{\tilde{D}}_{x,y} = 2[\cos(2k_c) - 1]D_{x,y}. \quad (22)$$

For our standard parameter set the coefficient δ is positive and hence, the Turing instability is subcritical confirming the presence of a hard excitation. Furthermore, we scanned the parameter space of the diffusion constants and found that δ is indeed always positive regardless of the values of D_x and D_y, thus excluding a supercritical bifurcation. We remark that in order to gain information on the resulting patterns we would have to extend the analysis to higher orders of the Ginzburg-Landau equation. However, this is beyond the aim of this study.

Summarizing the results obtained so far we have learned that the dichotomous switching has two effects on the extended system. First it induces a stable inhomogeneity in the form of isolated local activated regions, where isolated humps are built on the homogeneous background. Secondly it causes a transition between two coexisting stable states creating new humps with each switching. Our numerical simulations showed the stability of each of these multi hump states. Moreover, the eventually resulting perfectly periodic inhomogeneous steady (Turing pattern) turns out to be the most stable of all stationary states with respect to global switching. From an alternative point of view the global dichotomous switching entails the inhomogeneous steady state to grow at the cost of the homogeneous state.

FIG. 10. Instability of the boundary. We show successive snapshots of a 2000×2000 array with $\Delta r=0.02$ at $t=0$, $t=170$, and $t=705$. The pattern slowly evolves throughout the whole space. $a=1.475$.

IV. FROZEN NOISE

In this section we investigate the limit of vanishing switching rates of the random telegraph signal, i.e., in this way we incorporate static dichotomous disorder in the system. The spatial correlation of the random signal is governed by the lattice spacing used in our simulation. An example for the realization of static dichotomous disorder in a two-dimensional lattice system is depicted in Fig. 9. The right panel of Fig. 9 shows the results of a numerical simulation with that noise realization. As in the case of fast global switching we see a Turing pattern emerge. The pattern is not a mere reflection of the underlying disorder but has a structure of its own. Its typical wavelength is much larger than that of the disorder. As initial conditions we chose $x_i=0.56748$ and $y_i=0.384732$ for all $i=1,\ldots,N$. This is the location of the stable fixed point of a single system without dichotomous driving ($I_i=0$). The dynamical process of pattern formation is again driven by a Turing instability. Perturbations of a certain critical wavelength grow until they form the pattern shown in Fig. 9. The pattern formation takes place in 2D as well in 1D. Typically, Turing patterns in 2D come in two different shapes [18]: In labyrinth- and in hexagonal shape. With our study we found that the lattice system of Eqs. (1) and (2) supports only the labyrinth type.

As the influence of different correlation lengths of the disorder is concerned we have investigated numerically different samples with the same lattice constant but with frozen dichotomous signals of different typical wavelength. The implementation in our numerical computations proceeded as follows: For every run of our simulation we chose a different integer l. We randomly selected a value for the realization of I for the first element of the lattice system and applied this value to $l-1$ consecutive elements. We then picked a new I value independently of the first, applied it to the next l units, and so on. When the boundary of the grid is reached we apply the same realization of I to the $l-1$ consecutive lines. This procedure is repeated until the whole space is filled with squares of side length l that share a realization of I.

Until now we have dealt with the situation where the typical wavelength $l\Delta r$ of the disorder is much smaller than that of the pattern. Now we explore the opposite case: the typical wavelength is much larger than that of the pattern we have observed above. An example is given in Fig. 10.

As initial conditions we used $\dot{\mathbf{x}}_{0,\mathrm{det}}$. With coarse disorder (compared to the lattice spacing as well as to the pattern wave length) there arise sharp borders separating the ex-

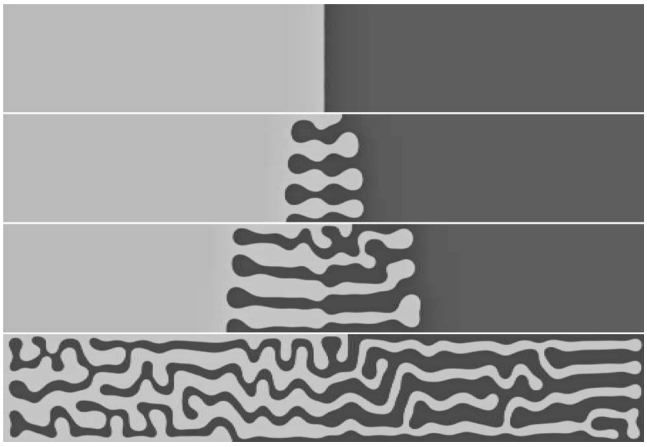

FIG. 11. Instability of a straight boundary. We show successive snapshots of a 500×3000 array with $\Delta r=0.2$ at $t=250$, $t=1357$, $t=2370$, and $t=4163$. The pattern slowly evolves throughout the entire space. $a=1.46$, $D_x=0.1$, $D_y=10$.

tended regions associated with the two different values of the static disorder. Units far from these borders feel little of the disorder and hence, get, as in a deterministic system, attracted by the fixed point connected with the local realization of I. The interface between the two regions at a corner is not stable, though. As the central and right panels in Fig. 10 reveal, fluctuations in the border region grow and expand into the homogeneous part of the pattern. Analogous phenomena have been reported for bistable media in Ref. [15]. This behavior goes on until the complete plane displays a patterned structure. As stated above this effect is not observable in the 1D system.

It is illustrative to examine cases with slightly different values of the parameter a. While for our standard parameter $a=1.475$ a flat border is stable and we need a corner for inhomogeneities to grow a slight change to $a=1.46$ destabilizes flat surfaces. This is shown in Fig. 11. Noteworthy this change of parameters goes along with a qualitative change of the topology of the system's phase space: Three limit cycles are born. Two of them are unstable and are centered around the stable fixed points. One is stable and envelops all fixed points and other limit cycles.

Particularly illuminating are simulations with the use of different correlation lengths in parameter regions where the homogeneous deterministic system $[I_i(t)=0]$ does not support Turing pattern formation. We therefore reduce the inhibitor coupling coefficient to $D_y=0.5$. In the deterministic system the homogeneous solution at the fixed points $x_{0,\mathrm{det}}$ is stable ($-x_{0,\mathrm{det}}$ as well). If we apply a very fine dichotomic noise realization, i.e., one with a small typical length $l\Delta r$ we find, as expected, a behavior equivalent to that of the deterministic system: a homogeneous distribution at the fixed point (upper row in Fig. 12). If we apply a coarser dichotomic perturbation we observe a behavior differing from that of the deterministic system: Stationary patterns form (lower line in Fig. 12). We can thus increase the parameter range in which Turing patterns emerge. We want to emphasize that the ratio between activator and inhibitor diffusion constant can be significantly decreased.

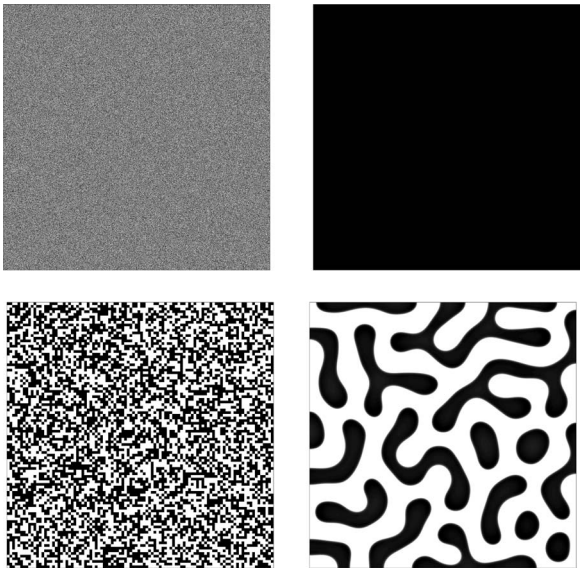

FIG. 12. Coarse fluctuations support pattern formation, fine ones do not. In this parameter regime the system with $I_i(t)=0$ does not support Turing pattern formation. $D_y=0.5$, $\Delta r=0.02$, $l=1$ (upper row) and $l=20$ (lower row). 2000×2000 points are shown.

A similar system with static dichotomous disorder has been studies experimentally in Ref. [34]. Here one of the two states that the dichotomous disorder produces exhibits Turing instability while the average value does not. For suitable correlation length of the fluctuations the authors report Turing pattern formation.

To gain some insight into the role of large correlation length of the disorder we computed its structure factor $S(k)$ in 1D. It is given by the Fourier transform of the spatial correlation function. The latter is computed as follows:

$$\langle I_i I_j\rangle = \sum_{I_i,I_j=+d,-d} I_i I_j p(I_i,I_j), \tag{23}$$

where $p(I_i,I_j)$ is the joint probability that I takes the value $\pm d$ at site i and $\pm d$ at site j. There are four different combinations for that but due to symmetry reasons it reduces to only two different values for p, one for equal realizations, and one for a realization with opposite signs.

These probabilities can be expressed in terms of conditional probabilities

$$\begin{aligned} p(I_i=+d,I_j=+d) &= p(i,j\in l_k)p(I_i=+d,I_j=+d;i,j\in l_k) \\ &+ p(i,j\notin l_k)p(I_i=+d,I_j=+d;i,j\notin l_k). \end{aligned} \tag{24}$$

Here $p(i,j\in l_k)$ is the probability that site i and site j are in the same interval (with index k; $k=1,\ldots,N/l$) of length l in which we fixed the value of I. $p(I_i=+d,I_j=+d;i,j\in l_k)$ denotes the conditional probability that I_i takes the value $+d$ and I_j takes the value $+d$ if the corresponding sites are in the same aforementioned interval. With our algorithm for constructing the frozen disorder of box length l the latter probability is equal to one half (one half for either sign of I). $p(I_i=+d,I_j=+d;i,j\notin l_k)$ is equal to one forth. $p(i,j\in l_k)$ can be calculated as follows: The probability that randomly chosen elements that are further apart than the length of an

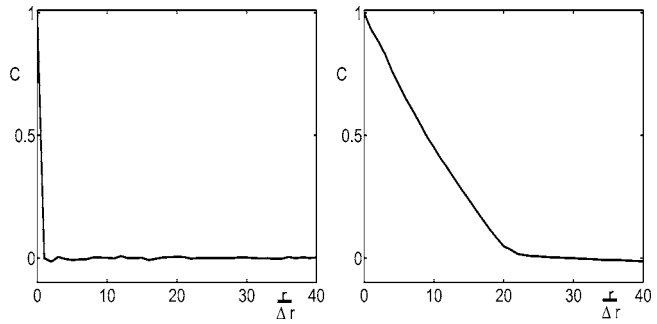

FIG. 13. Autocorrelation of the noise $C=\langle I_i I_j\rangle$ where the sites i and j are r apart over the distance r. The left panel corresponds to the upper noise realization in Fig. 12, the right panel to the lower one.

interval belong to the same interval is zero. If they are closer than that, the probability that the border between two intervals lies between the two elements, is given by

$$p(i,j \notin l_k) = \frac{|i-j|}{l}, \quad |i-j| < l. \tag{25}$$

The elements with sites i and j are then not in the same interval. $p(i,j \in l_k)=1-p(i,j \notin l_k)$ is the complementary probability.

With this we are able to compute

$$\langle I_i I_j\rangle = d^2\left(1 - \frac{|i-j|}{l}\right) \tag{26}$$

and we finally arrive at

$$S(k) = \frac{2d^2}{lk^2}[1-\cos(kl)]. \tag{27}$$

We show a plot of the 2D autocorrelation function in Fig. 13 and the averaged 1D power spectrum in Fig. 14.

Note that the power at the critical wave number k_c is much higher in the case of a large correlation length of the disorder than for small correlation length. This is a possible reason for the formation of the patterns. The high power at k_c may lead to a larger amplitude of the deviations from the steady state of wavelength k_c and drive the system further into the nonlinear regime.

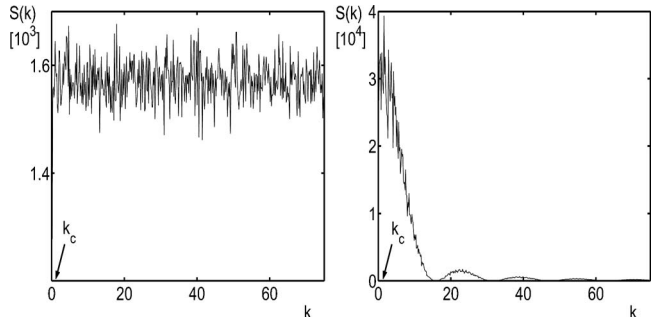

FIG. 14. Structure factor $S(k)$ of the underlying noise for the patterns in Fig. 12. The left panel corresponds to the fine disorder in Fig. 12 (upper row), the right to the coarse disorder (lower row).

V. CONCLUSIONS

We have investigated the influence of dichotomous fluctuations on pattern formation in a diffusively coupled extended FHN system. The fluctuations were chosen such that locally one of two excitable dynamics was realized at a certain time. We emphasize that in both dynamics there exists one stable homogeneous steady state. We have shown that due to appropriate switching between the two dynamical regimes either of the two steady states can be destabilized.

For global switching depending on the corresponding rate we found tree different mechanism for the creation of Turing patterns: For very fast (global) switching (compared to the activation time of the FHN) the parameter regime at which the destabilization takes place coincides with those values for which Turing instability occurs in the system with applied mean value of the fluctuations ($I=\langle I\rangle=0$).

For slow switching Turing patterns can be found likewise. Here existing inhomogeneities are necessary for their formation. The boundaries of the inhomogeneities are unstable and a pattern slowly evolves from them into the homogeneous part.

In the case of global alterations of intermediate switching rate γ (comparable to the inverse activation time) we found a new mechanism to create spatial structures: If one switching occurs at the correct time stable local inhomogeneities are formed. Further switchings lead to a growth of the inhomogeneous regions at the boundary to the homogeneous regions. The pattern is in that sense more stable with respect to slow global alteration of the dynamics than the homogeneous state. Investigation of the stationary solutions of the system with the help of a nonlinear map approach yields bistability of a period-one and a period-two orbit corresponding in real space to the homogeneous and the Turning pattern state, respectively. After a stable spatial inhomogeneity is formed both of these states coexist in the extended system. The regions are coupled via diffusion terms. The effect of further switching is then to enlarge the region of inhomogeneity on the expense of the homogeneous region. We remark that a change of the parameters reverses the process back to the overall homogeneous state.

Applying frozen dichotomous disorder of finite nonzero correlation length causes destabilization of homogeneous steady states leading again to Turing patterns. In the limit of small correlation length the averaging over the realizations ($I(r)=\langle(\ )I\rangle=0$) works very accurately, too.

For larger correlation length homogeneous regions can be destabilized for parameters that for $I=0$ as performed in Ref. [30] do not allow for a Turing instability. In particular in our case no strong deviation between the diffusion constants of the activator and inhibitor is needed.

The case of large correlation length is equivalent to the limit of slow global switching in systems with existing inhomogeneities: Boundaries between regions of distinct realizations of I become unstable and a pattern evades into the homogeneous part.

We also performed investigations with fluctuations varying in both space and time. Since the labyrinth pattern is stable against any realization of the disorder (at least for our

noise strength) such a pattern persists once established.

If the spatial disorder initiates pattern creation and the inverse switching frequency is higher than the evolution time a pattern will typically be created before the next switching occurs. The next realization of the disorder will have hardly any impact on the once established pattern. There will therefore be no systematic influence of the temporal fluctuations.

On the other hand if we look at large spatial correlations and fast switching times we note that the time it takes for the pattern to evolve from the boundaries of a pattern with very coarse spatial disorder (see Fig. 10) into the homogeneous regions is also much larger than the typical evolution time of a labyrinth pattern caused by fast switching. This phenomenon will therefore have only little effect on the resulting pattern.

In the case of very fast switching and very small typical wavelength of the disorder the dynamics of the system average out the fluctuations just as it is the case with high spatial or temporal switching rates, only. It is only in the case of intermediate spatial and temporal switching rates that both effects have an influence on the system. We find that the spatial and temporal disorder usually provides the right conditions for inhomogeneities to grow at an earlier time and at more sites in the system and thereby speeds up the pattern formation.

Adding a spatial or temporal component to the fluctuations assists the system to average them out. Therefore the effect of enhancing Turing pattern formation by a certain typical wavelength (see Fig. 12) is disabled by high switching rates.

ACKNOWLEDGMENTS

This work was supported by SFB-555 and the VW Foundation project No. I/80425.

APPENDIX: A STANDING LOCALIZED PATTERN SOLUTION—NONLINEAR MAP APPROACH

We demonstrate how a standing localized single hump is represented by the solution of the stationary system. To this end we utilize a nonlinear map approach [35,36]. Inserting into Eqs. (1) and (2) $\dot{x}_n=\dot{y}_n=0$ results in the difference system

$$x_i - x_i^3 - y_i + D_x \frac{x_{i+1} - 2x_i + x_{i-1}}{(\Delta r)^2} = 0, \tag{A1}$$

$$x_i - a y_i + \hat{D}_y \frac{y_{i+1} - 2y_i + y_{i-1}}{(\Delta r)^2} = 0, \tag{A2}$$

with $\hat{D}_y = D_y/\epsilon$. In addition we have introduced the lattice spacing Δr. Bearing in mind that $D_x/D_y \ll 1$ the problem can be divided into two separate problems (the inner and outer problem, respectively) each having solution varying on its own spatial scale. After having constructed the partial solutions they must be connected with suitable matching and boundary conditions, respectively. The procedure is equivalent to the study in the corresponding continuum models (see, e.g., Ref. [37]). First there is the region on the lattice in which x_n alters so rapidly on the short scale of order $\sqrt{D_x}$ that the diffusion term $D_x[x_{i+1}-2x_i+x_{i-1}]/(\Delta r)^2$ can balance the other terms in Eq. (A1) even with a small value of D_x. Stretching of the length scale according to $\Delta r' = \Delta r/\sqrt{D_x}$ the rescaled system reads

$$x_i - x_i^3 - y_i + \frac{x_{i+1} - 2x_i + x_{i-1}}{(\Delta r')^2} = 0,$$

$$x_i - a y_i + \frac{\hat{D}_y}{D_x} \frac{y_{i+1} - 2y_i + y_{i-1}}{(\Delta r')^2} = 0. \tag{A3}$$

Since $\hat{D}_y/D_x \gg 1$ the leading order system reduces to

$$x_i - x_i^3 - y_i + \frac{x_{i+1} - 2x_i + x_{i-1}}{(\Delta r')^2} = 0,$$

with constant y_i. Taking into account the symmetry properties of the solution the last equation can be satisfied with $y_n=0$ so that the first equation reduces to $x_i - x_i^3 - y_i + (x_{i+1} - 2x_i + x_{i-1})/(\Delta r')^2 = 0$. With the notation $x_n = u_n$ and $x_{n-1} = v_n$ the difference equation can be cast into mapping form

$$u_{n+1} = u_n^3 - u_n - v_n, \quad v_{n+1} = u_n.$$

On the $u-v$ plane the map possesses a heteroclinic connection related to a pair of hyperbolic fixed points at $(\pm 1, \pm 1)$. The origin constitutes an elliptic fixed point [35,36]. On the lattice the heteroclinic connection establishes a kinklike profile corresponding to the steep border of the hump.

Outside the boundary layer x_n varies on the same scale as y_n and the term $D_x[x_{i+1}-2x_i+x_{i-1}]/(\Delta r)^2$ in Eq. (A1) can be discarded. The leading order system is then given by

$$0 = x_i - x_i^3 - y_i, \tag{A4}$$

$$0 = x_i - a y_i + \hat{D}_y \frac{y_{i+1} - 2y_i + y_{i-1}}{(\Delta r)^2}. \tag{A5}$$

The cubic equation (A4) can be readily solved for $x=x(y)$ by approximating linearly on the left and right branches of the cubic nullclines around $y=0$. This yields $x_\pm = \pm 1 - y/2$ which upon inserting into Eq. (A3) results in the linear difference equations $[\pm 1 - (1/2 + a) y_i] + \hat{D}_y [y_{i+1} - 2y_i + y_{i-1}]/(\Delta r)^2 = 0$. The general solution of this equation reads

$$y_n = C_1^{\pm} \exp(\kappa n) + C_2^{\pm} \exp(-\kappa n), \tag{A6}$$

with exponent $\kappa = \cosh^{-1}[1 + (a + 1/2)\epsilon D_y]$. The coefficients $C_{1,2}^{\pm}$ are determined from the boundary conditions as well as the matching conditions.

[1] A. S. Mikhailov, *Foundations of Synergetics I*, 2nd ed. (Springer, Berlin 1994).
[2] J. Garcia-Ojalvo and J. M. Sancho, *Noise in Spatially Extended Systems* (Springer-Verlag, New York, 1999).
[3] V. Anishchenko, A. Neiman, A. Astakhov, T. Vadivasova, and L. Schimansky-Geier, *Chaotic and Stochastic Processes in Dynamic Systems* (Springer, Berlin 2002).
[4] A. S. Mikhailov, Z. Phys. B: Condens. Matter **41**, 277 (1981).
[5] J. Garca-Ojalvo, J. M. Sancho, and L. Ramirez-Piscina, Phys. Lett. A **168**, 35 (1992).
[6] J. Garca-Ojalvo, A. Hernndez-Machado, and J. M. Sanchol, Phys. Rev. Lett. **71**, 1542 (1993).
[7] A. Becker and L. Kramer, Phys. Rev. Lett. **73**, 955 (1994).
[8] J. M. R. Parrondo, C. van den Broeck, J. Buceta, and F. J. de la Rubia, Physica A **224**, 153 (1996).
[9] A. A. Zaikin and L. Schimansky-Geier, Phys. Rev. E **58**, 4355 (1998).
[10] J. Buceta, M. Ibanes, J. M. Sancho, and K. Lindenberg, Phys. Rev. E **67**, 021113 (2003).
[11] V. Beato, I. Sendia-Nadal, I. Gerdes, and H. Engel, Phys. Rev. E **71**, 035204 (2005).
[12] B. Lindner, J. Garcia-Ojalvo, A. Neiman, and L. Schimansky-Geier, Phys. Rep. **392**, 321 (2004).
[13] R. FitzHugh, Biophys. J. **1**, 445 (1961).
[14] J. Nagumo, S. Arimoto, and S. Yoshitzawa, Proc. IRE **50**, 2061 (1962).
[15] C. Elphick, A. Hagberg, and E. Meron, Phys. Rev. E **51**, 3052 (1995).
[16] K. Martinez, A. L. Lin, R. Kharrazian, X. Sailer, and H. L. Swinney, Physica D **168**, 1 (2002).
[17] A. Hagberg and E. Meron, Nonlinearity **7**, 805 (1994).
[18] A. J. Koch and H. Meinhardt, Rev. Mod. Phys. **66**, 1481 (1994).
[19] J. D. Murray, *Mathematical Biology*, 2nd ed. (Springer-Verlag, New York, 2003).
[20] R. Kawai, X. Sailer, L. Schimansky-Geier, and C. Van den Broeck, Phys. Rev. E **69**, 051104 (2004).
[21] J. Buceta, K. Lindenberg, and J. M. R. Parrondo, Phys. Rev. Lett. **88**, 024103 (2002).
[22] J. Buceta, K. Lindenberg, and J. M. R. Parrondo, Phys. Rev. E **66**, 036216 (2002).
[23] J. Buceta and K. Lindenberg, Phys. Rev. E **66**, 046202 (2002).
[24] S. Koga and Y. Kuramoto, Prog. Theor. Phys. **63**, 106 (1980).
[25] J. Rinzel and J. B. Keller, Biophys. J. **13**, 1313 (1973).
[26] T. Ohta, M. Mimura, and R. Kobayashi, Physica D **34**, 1115 (1989).
[27] T. Ohta, A. Ito, and A. Tetsuka, Phys. Rev. A **42**, 3225 (1990).
[28] M. Kaern, R. Satnoianu, A. P. Muuzuri, and M. Menziger, Phys. Chem. Chem. Phys. **4**, 1315 (2002).
[29] G. P. Harmer and D. Abott, Nature (London) **199**, 402 (1999).
[30] J. Buceta and K. Lindenberg, Phys. Rev. E **68**, 011103 (2003).
[31] P. Manneville, *Dissipative Structures and Weak Turbulence* (Academic Press, San Diego, 1990).
[32] Y. Kuramoto, *Chemical Oscillations, Waves, and Turbulence* (Dover, Mineola, NY, 2003).
[33] X. Sailer, Dissertation Humboldt Universität zu Berlin (in preparation).
[34] A. Sanz-Anchelerues, A. M. Zhabotinsky, I. R. Epstein, and A. P. Muuzuri, Phys. Rev. E **63**, 056124 (2001).
[35] D. Hennig, K. Ø. Rasmussen, H. Gabriel, and A. Bülow, Phys. Rev. E **54**, 5788 (1996).
[36] D. Hennig and G. P. Tsironis, Phys. Rep. **307**, 333 (1999).
[37] P. C. Fife, SIAM-AMS Proc. **10**, 23 (1976).